Chemical Engineering Journal 166 (2011) 631–638

Contents lists available at ScienceDirect

Chemical Engineering Journal

journal homepage: www.elsevier.com/locate/cej

Removal of aqueous toxic Hg(II) by synthesized TiO_2 nanoparticles and TiO_2/montmorillonite

Binlin Dou [a,b], Valerie Dupont [b,*], Weiguo Pan [c], Bingbing Chen [c]

[a] Key Laboratory of Ocean Energy Utilization and Energy Conservation of Ministry of Education, Dalian University of Technology, 116023 Dalian, China
[b] Energy & Resources Research Institute, University of Leeds, Leeds LS2 9JT, UK
[c] School of Energy and Environment Engineering, Shanghai University of Electric Power, Pingliang Rd. 2103, 200090 Shanghai, China

ARTICLE INFO

Article history:
Received 3 September 2010
Received in revised form 5 November 2010
Accepted 8 November 2010

Keywords:
TiO_2
Montmorillonite
Hg(II) removal
Photocatalyst
Aqueous solution

ABSTRACT

The adsorption and photocatalytic reduction of toxic Hg(II) in aqueous solutions were investigated at different temperatures using synthesized TiO_2 nanoparticles and TiO_2/montmorillonite. The synthesized materials were tested by TGA, BET, TEM and XRD methods. High-purity anatase TiO_2 nanoparticles with an average diameter of 9.10 nm were produced by the acid catalyzed sol–gel method at 500 °C, and the specific surface area of synthesized TiO_2 nanoparticles was in excess of 200 $m^2\,g^{-1}$. TiO_2/montmorillonite was prepared by slurry reactions, resulting in average pore size of 3.10 nm with TiO_2 nanoparticles on the montmorillonite surface. TiO_2/montmorillonite with a 22 wt% TiO_2 load exhibited a specific surface area of 239 $m^2\,g^{-1}$. Removal of Hg(II) in aqueous solutions at 25, 35 and 45 °C in darkness and under UV illumination showed that the photocatalytic reduction of Hg(II) increased with increasing temperature, and a decline in adsorption was observed for a rise in temperature from 25 to 45 °C, following the exothermicity of the adsorption process. The adsorption behavior of Hg(II) on TiO_2 nanoparticles was well described by the Langmuir isotherm model, and the rates were simulated by the Elovich equation. A first-order reaction model was used to simulate the photocatalytic reduction reaction of Hg(II) in aqueous solutions, and a good fit was obtained with the experimental data.

1. Introduction

The Hg(II) in industrial wastewaters has received increasing attention as a serious pollutant due to its toxic and bioaccumulative properties [1,2]. In aquatic systems, Hg(II) are often converted by bacteria to methylmercury. When local conditions exacerbate this process, it poses a health risk to humans and wildlife through the aquatic food chain [2]. As Hg(II) in excess of 0.5 ng ml^{-1} could significantly increase alkylation of the element in water bodies, and subsequently threaten all forms of sustainable development, many states have enacted legislation with the goal of reducing mercury emissions to air, land and water. Several methods have been studied for the removal of Hg(II) in aqueous solutions including activated carbon adsorption, ion-exchange, precipitation and photocatalytic reduction [1–8]. The adsorption and photocatalytic reduction techniques by TiO_2 materials appear to be most promising because of their high efficiency and simplicity of operation. More importantly, Hg(II) can be removed from the solution by photocatalytic reduction with TiO_2 to elemental mercury which can be safely recovered [5]. Some studies indicated that nanosized TiO_2 offered several advantages over the commercially available (e.g. Degussa) TiO_2: a high surface area for reactions to occur; and introduction of deeper trapping sites outside the TiO_2 particle resulting in greater separation of photogenerated charges and enhanced reduction properties of photogenerated electrons [6]. Some studies have illustrated the adsorption and photocatalytic reduction of Hg(II) by the TiO_2 powders and only the effect of solution pH has been covered [2,6,7].

TiO_2 can exist in three crystalline modifications: rutile (tetragonal), anatase (tetragonal), and brookite (orthorhombic). Although the studies showed the effect of rutile TiO_2 on the photocatalytic reduction of Hg(II) in aqueous systems [7,8], anatase TiO_2 is a very active allotropic when nano-sized. Anatase TiO_2 nanoparticles generally display unique properties, such as quantum size effect, high surface area and short interface migration distance, all of which achieve enhanced photocatalytic performance [9–11]. Many methods such as solution phase synthesis [12–14], chemical vapor deposition [15,16], flame synthesis [17,18], the alkoxide sol–gel method [9,19–21], and others [22] have been developed to synthesize anatase TiO_2 nanoparticles. It is well known that nanoparticles have a strong tendency to aggregate in concentrated state, and the aggregation of TiO_2 nanoparticles would lead to the decrease in active surface area of the catalyst, resulting in the decrease in catalytic activity. The anatase phase is also thermodynamically

* Corresponding author. Tel.: +44 113 3432503; fax: +44 113 2467310.
E-mail address: v.dupont@leeds.ac.uk (V. Dupont).

1385-8947/$ – see front matter
doi:10.1016/j.cej.2010.11.035

less stable than the rutile phase, and its formation is kinetically favored at lower temperature. Thus, it is not easy to synthesize TiO_2 nanoparticles with high surface area, narrow size distribution and uniform anatase crystalloid [23,24]. In addition, the synthesis apparatus and product separation should be uncomplicated preferably for low-cost commercial applications [25,26].

Recently, TiO_2 composites have also been studied by preparing a series of compounds such as microcrystalline TiO_2 pillared clays, mixed Ti/Si, Ti/V oxides, nanocrystals of TiO_2 dispersed in inorganic media [27–33]. Some studies indicated that TiO_2 supported on porous adsorbents is a potential catalyst system for the continuous removal of contaminants from wastewaters [30,34]. Especially, TiO_2/montmorillonite has been attracting much attention as a new low-cost type of photocatalyst, since its high surface area and superior properties accelerate photocatalytic reactions [31,34].

The aim of the present investigation is to study the adsorption and photocatalytic reduction of Hg(II) in aqueous solutions by synthesized TiO_2 nanoparticles and TiO_2/montmorillonite. The synthesized materials were characterized by TGA, BET, TEM and XRD. The effects of solution temperatures on the removal of Hg(II) in aqueous solutions were tested. The adsorption equilibrium at different temperatures was studied by the Langmuir isotherm model. The kinetic models of adsorption and photocatalytic reduction were tested with the experimental data.

2. Experimental

2.1. Materials

2.1.1. Preparation of TiO_2 nanoparticles

We tried to synthesize TiO_2 nanoparticles by applying a controlled acid catalyzed sol–gel method using HNO_3, ethanol and titanium alkoxides, which enables the synthesis of oxide particles with a regulated particle growth through a gel state [24,34–36]. The sol was prepared using HNO_3, ethanol and titanium alkoxides following the hydrolysis reaction of the Ti precursor in the solution with the temperature of 60–80 °C and the pH of 2–4. The molar ratio of $Ti(OC_4H_9)_4$, ethanol, HNO_3 and deionized water was maintained at 1:20:0.05:3. $Ti(OC_4H_9)_4$ was added dropwise into the mixture solution of ethanol, HNO_3 and deionized water under continuous stirring for 2 h with ultrasonic vibration treatment, and a homogeneous pale yellow-green solution was obtained. This was allowed to age at room temperature for 48 h and then dried in an oven at 80 °C for 12 h. It was then calcined in ambient atmosphere at 500 °C for 2 h in a conventional furnace.

2.1.2. Preparation of TiO_2/montmorillonite

Some studies reported the preparation of TiO_2/montmorillonite [27,31,32,37]. Typically, 40 ml of $Ti(OC_4H_9)_4$ were added dropwise into 250 ml of ethanol. The mixture was then added gradually to the HNO_3 solution of 1 mol l^{-1} under continuous stirring for 2 h to produce a transparent solution. Subsequently, the pH was adjusted to 2.5 with the addition of 1 mol l^{-1} NaOH resulting in a turbid colloid. The molar ratio of ethanol, $Ti(OC_4H_9)_4$ and HNO_3 was 12:5:1.6. The montmorillonite used in this study was the sodium-exchanged bentonite. The cation exchange capacity was 83 meq. per 100 g, followed by a washing-centrifugation procedure to make the supernatant nearly A sample of 10 g of montmorillonite was firstly saturated with water for 0.5 h, and mixed with cetyltrimethylammonium bromide (CTAB) and (DDA) [38]. This was then mixed with a given amount of TiO_2 sol, stirred for 1 h with treatment-neutral ultrasonic vibration. The mixture was dried for 24 h at 80 °C, calcined at 500 °C for 2 h in a conventional furnace.

2.2. Characterization

The synthesized materials were tested using different techniques. The thermal decomposition behavior of material precursors was examined using a thermo-gravimetric analyzer (model SDT 2960 and thermal analyst 2000, TA instruments). The specific surface areas were determined with the BET method using a Micrometric Acusorb 2100E apparatus. The TiO_2 nanoparticles size was measured by Transmission Electron Microscope (TEM; JEM 4010). The TiO_2 content in the TiO_2/montmorillonite was determined by elemental analysis using X-ray fluorescence method (Rigaku Industrial Corporation, RIX-2000). The X-ray powder diffraction spectra of materials were analyzed using a Shimadzu XRD-6000 powder diffractometer, where a Cu target Ka-ray (operating at 40 kV and 30 mA) was used as the X-ray source. The particles diameter was also estimated by Scherrer's equation.

2.3. Removal of Hg(II) in aqueous solutions

The experiments of Hg(II) removal were carried out in a cylindrical glass reactor containing 200 ml of Hg(II) solutions with the temperature control and a magnetic stirrer. Stock solutions of Hg(II) were prepared by dissolving analytical grade $HgCl_2$ in deionized water, and initial concentrations (c_0) were adjusted to 100 mg l^{-1} for each experiments. The pH values of $HgCl_2$ solutions were adjusted to 6.0 by hydrochloric acid. The experimental approach was similar to those reported in the literature [2,5,39]. A mass of 2 g of the synthesized materials was used for the tests of Hg^{2+} removal in dark conditions as well as for the tests under UV irradiation by a water-cooled 125 W medium pressure mercury lamp. During the experiments, samples were collected at selected time intervals. In a typical photocatalytic reduction run, the catalyst was suspended in the solution in the dark for 2 h by stirring to reach a given adsorption capacity prior to the photo-reduction experiment under UV irradiation. The Hg(II) concentrations (c, mg l^{-1}) in aqueous solutions were analyzed by Cold Vapor Atomic Absorption Spectrometry (CVAAS). In a typical run, the catalyst of TiO_2 nanoparticles was suspended in the solutions and the solutions were continuously stirred for enhanced diffusion and reaction. Because of the extreme sensitivity of the analytical procedure and the presence of mercury in a laboratory environment, care was taken to avoid extraneous contamination. Sampling devices, sample containers and plastic items were free of any form of mercury contaminants. The spent materials after experiments were safely kept and treated according to the laboratory regulation.

3. Results and discussion

3.1. Characterization of TiO_2 nanoparticles and TiO_2/montmorillonite

The TGA results of the precursors of the two materials before calcination are shown in Fig. 1. The main mass loss value was about 14–17% below 500 °C for TiO_2 nanoparticles. The DTG curve showed decomposition peaks at 350 °C, which may be due to the removal of chemisorbed water and structural hydroxyl groups. The TGA curve of the TiO_2/montmorillonite showed a significant mass loss in the region of 200–450 °C with a maximum at 310 °C from DTG curve, caused by the decomposition of surfactant molecules and the removal of structural hydroxyl groups. The results also indicated the exchange of Na^+ ions with the bulky organic cations CTA^+ in the clay mineral [40–42]. The organic matter degradation in the precursor of TiO_2/montmorillonite is mainly based on C_xH_y decomposition, and water and CO_2 are continuously released, resulting in increase of the basal spacing in layer structure [37,38,40]. The

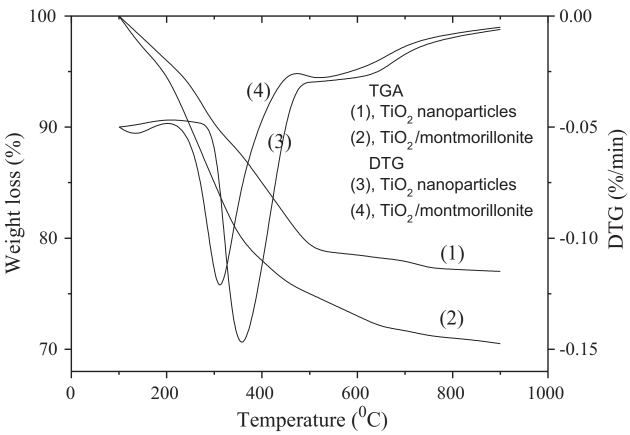

Fig. 1. TG-DTG curves of the two material precursors.

Table 1
Properties of the two materials synthesized.

Material	Specific surface area ($m^2\,g^{-1}$)	Pore volume ($cm^3\,g^{-1}$)	Avg. pore size (nm)
TiO_2 nanoparticles	210.1	0.213	0.082
TiO_2/montmorillonite	239.0	0.558	3.10

specific surface area, pore diameter and pore volume for the two materials were determined using nitrogen adsorption/desorption isotherm and multi-point BET analysis, the results of which are shown in Table 1. It can be seen that the specific surface area of the TiO_2 nanoparticles was higher than 200 $m^2\,g^{-1}$. A significant result was that the TiO_2/montmorillonite exhibited the larger specific surface area of 239 $m^2\,g^{-1}$. The synthesized materials were tested and characterized by powder XRD analysis. All peaks of XRD patterns of the TiO_2 nanoparticles can be indexed to anatase TiO_2. They were in good agreement with the standard spectrum (JCPDS no.: 21-1272), and no significant peaks of rutile and brookite were observed. The TiO_2 characteristic reflections were observed from the XRD pattern of TiO_2/montmorillonite. Table 2 shows that the TiO_2 content of 22 wt% in the TiO_2/montmorillonite was dramatically higher than that in the purified montmorillonite. The XRD pattern of the pure montmorillonite showed reflections at 2θ = 6.820, 18.921,

Table 2
Chemical compositions of the purified montmorillonite and TiO_2/montmorillonite, (wt%).

Material	SiO_2	Al_2O_3	TiO_2	CaO	MgO	Na_2O	Others
Purified montmorillonite	69.8	12.5	0.1	3.0	3.3	2.6	8.7
TiO_2/montmorillonite	55.5	9.1	22.0	0.5	1.9	0.3	10.7

28.316°. The XRD patterns of the TiO_2/montmorillonite exhibited one diffraction line in the low angle range at 2θ = 3.168°, which corresponded to a layer spacing expansion [40]. TEM micrographs of the TiO_2 nanoparticles and the TiO_2/montmorillonite (Fig. 2) indicated that the TiO_2 nanoparticles obtained by the acid catalyzed sol–gel method were highly dispersed and without great aggregation. Montmorillonite layered silicates exist as platelets of 2-to-1 with a central row of silicate octahedral, flanked by two inward-pointing rows of magnesia or alumina. As can be seen from Fig. 2(b), the TEM patterns of the TiO_2/montmorillonite showed a cross-linked layer structure, and an aggregated oxide nanoparticles structure is also observed on the surface. Hydrolysis of $Ti(OC_4H_9)_4$ results in formation of either TiO_2 nanoparticle that heterogeneously nucleate on the montmorillonite surface to form a shell, or some nanoparticles that homogeneously nucleate to form a larger nanoparticle. The particles are included in the layer structure and have less than 3.1 nm size, while others with larger size were not present in the interlamellar spacing of the montmorillonite, and heterogeneously deposited on the external surface [40,41].

3.2. *Formation mechanisms of TiO_2 nanoparticles and TiO_2/montmorillonite*

It is interesting to note that the synthesized TiO_2 nanoparticles in this work were uniform anatase, and their size was quite small. It was mentioned earlier that anatase is a thermodynamically less stable phase than rutile. Its formation is typically favored at temperatures of less than 600 °C [29,42]. This lower temperature could explain the high surface area of the catalysts. The hydrolysis/polycondensation model for the formation of titanium dioxide from the reaction of titanium alkoxides with water in solution phase was shown in some studies [21,42–44]. It is not difficult to understand the enhancement effect of solution pH value in the

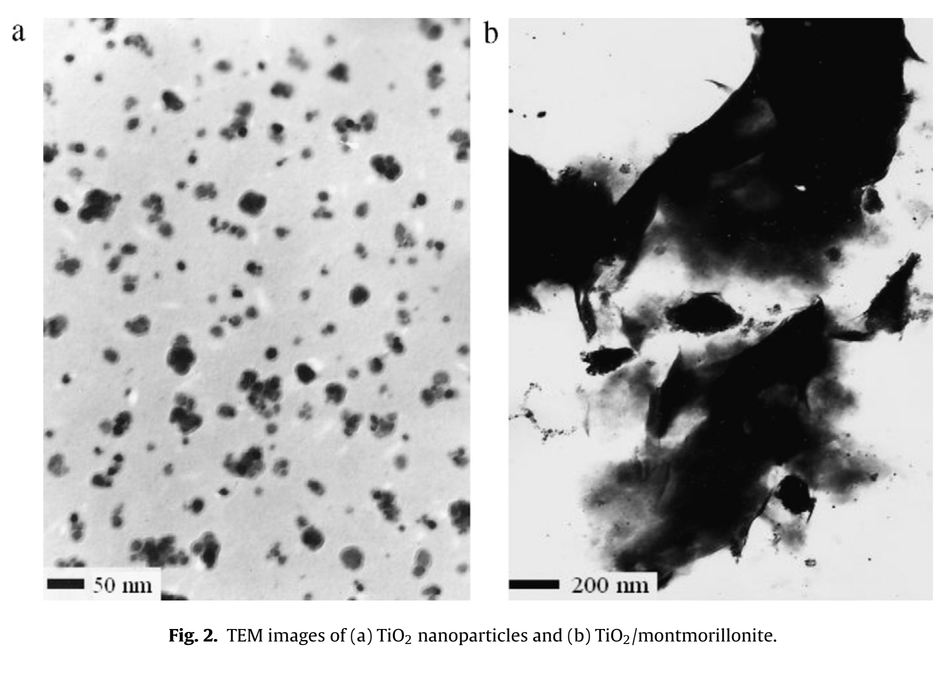

Fig. 2. TEM images of (a) TiO_2 nanoparticles and (b) TiO_2/montmorillonite.

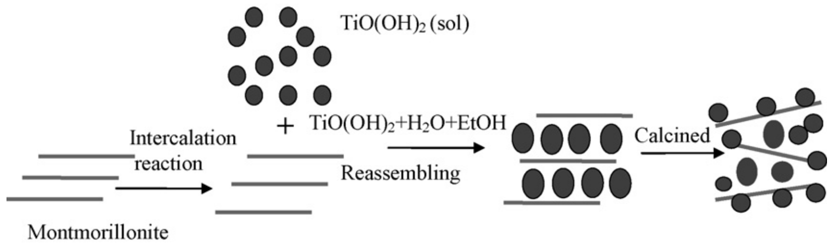

Fig. 3. Schematic diagram of the preparation method of TiO_2/montmorillonite.

overall hydrolysis reaction. The dehydroxylation and the dealcoholation are accelerated by acid to increase the overall surface hydrolysis process [44]. During this acid catalyzed sol–gel process, both the formation of sol particles and the gelation process took place, which increased the local pH, resulting in the hydrolysis of the Ti precursor, and created a dispersion of colloidal particles [21,42–44]:

$$TiO^{2+} + 2OH^- \rightarrow TiO(OH)_2(sol) \quad (R1)$$

Further reaction caused bonds to form between sol particles, resulting in a network of titanium oxyhydroxide gel [44]:

$$TiO(OH)_2(sol) - xH_2O \rightarrow TiO_{1+x}(OH)_{2-2x}(gel) \quad (R2)$$

Therefore, the nanoparticles by sol–gel preparation had very small sizes, small pores and single dispersal, preventing agglomeration.

The possible formation mechanism of mesoporous TiO_2/montmorillonite includes the intercalated quaternary ammonium cations and neutral amines as co-surfactants to direct the interlamellar hydrolysis and condensation polymerization of neutral inorganic precursor [31,38,40,45]. Thus the pore size becomes controllable, and the thermal stability is improved. The montmorillonite has also been proved to be a suitable host clay material for the controlled syntheses of catalytically active transition metal particles [31,34,45]. Unlike commonly reported microporous pillared structure, a TiO_2 cluster structure in the present study was observed. The purified montmorillonite was firstly modified by cetyltrimethylammonium bromide (CTAB) through an ion-exchange reaction [38,46]. The basal spacing was further expanded by the intercalation of dodecylamine (DDA). TiO_2 was dispersed and attached in the structure and surface of montmorillonite by hydrolyzing $TiO(OH)_2$ sol using $Ti(OC_4H_9)_4$ as the precursor. Fig. 3 shows a schematic of the preparation of TiO_2/montmorillonite. The low hydrolysis reaction results in the formation of smaller, uniform titanium hydrate and fine TiO_2 particles. The amount of TiO_2 introduced and remaining in the montmorillonite depends on the duration of impregnation and/or the ion exchange procedure. The general schemes for the production of functional nano-structured materials based on delaminated layered silicate particles have also been discussed by some investigators [31,33,47].

3.3. Removal of Hg(II) in aqueous solutions

A series of experiments of Hg(II) removal from aqueous solutions by two materials in the dark and under UV illumination were carried out at different temperatures. It should be noticed that it may take long time to reach saturation for adsorption of mercury(II) on the TiO_2 surface. The experiments in darkness indicated the adsorption of Hg(II) onto the surface of materials. Under the UV illumination, the removal of Hg(II) in aqueous solutions was related to photocatalytic reduction reaction.

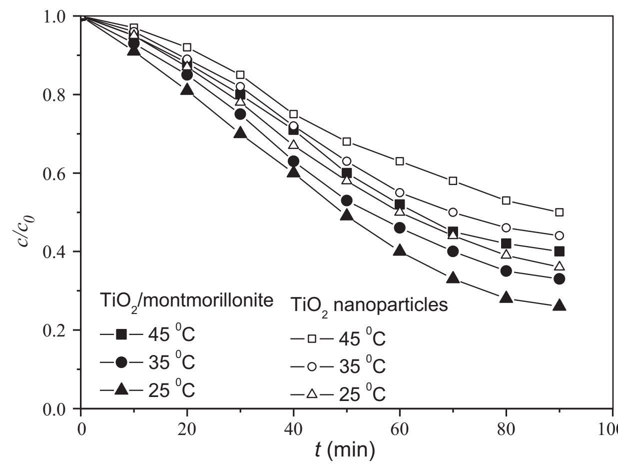

Fig. 4. Decreasing Hg(II) concentrations with time by adsorption at the different temperatures in aqueous solutions.

3.3.1. Adsorption of Hg(II)

The experimental results of the adsorption of Hg(II) onto the materials at different times are shown in Fig. 4. The results showed that the amount of Hg(II) adsorbed decreased with increasing temperatures and that TiO_2/montmorillonite had a higher adsorption activity compared to that of the TiO_2 nanoparticles. The higher adsorption capacity by TiO_2/montmorillonite could be attributed to its high BET surface area and the fact that the TiO_2 nanoparticles were attached on surface. Hg(II) equilibrium adsorption isotherms on the TiO_2 nanoparticles and TiO_2/montmorillonite are presented in Fig. 5 for different temperatures. The adsorption behaviors of Hg(II) on the solid materials may be described by the Langmuir

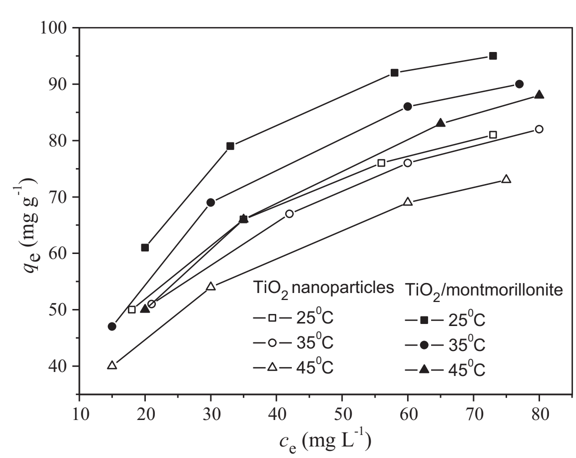

Fig. 5. Experimental equilibrium results of the adsorption of Hg(II).

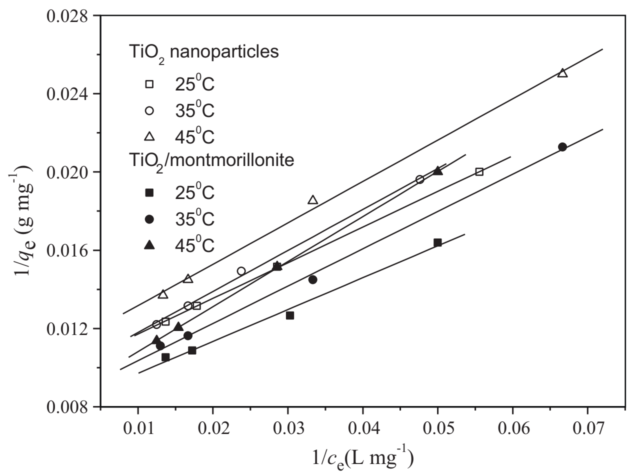

Fig. 6. Fitting results of the Langmuir isotherm model.

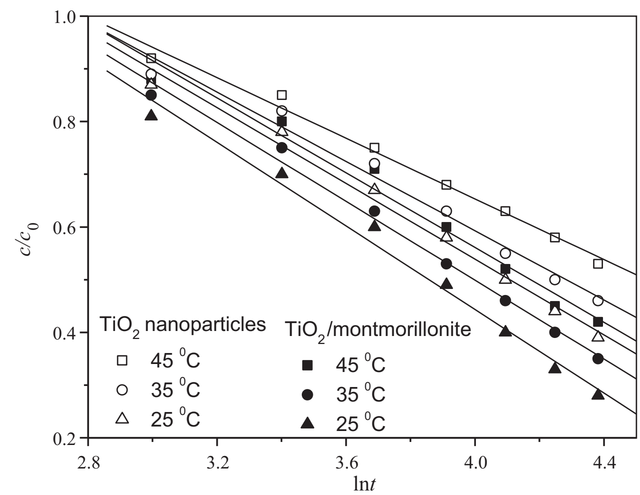

Fig. 7. Relationship of c/c_0 and $\ln t$ in the adsorption of Hg(II).

adsorption model:

$$q_e = \frac{Q^0 K_L c_e}{1 + K_L c_e} \tag{1}$$

where Q^0 (mg g^{-1}) and K_L (l mg^{-1}) are the Langmuir parameters, related with the maximum capacity of adsorption and with the binding energy of adsorption, respectively; c_e and q_e are the equilibrium liquid-phase concentration of Hg(II) and capacity of solid sample, respectively.

From the corresponding Langmuir parameters, the dimensionless parameter r or separation factor could be calculated following:

$$r = \frac{1}{1 + K_L c_0} \tag{2}$$

According to the calculated r values, $r = 0$ corresponds to irreversible adsorption, $0 < r < 1$ to the favorable equilibrium, $r = 1$ to the linear case and $r > 1$ to unfavorable equilibrium [48,49].

The Langmuir isotherm adsorption assumes that ions are adsorbed on definite sites that are monoenergetic on the sorbent surface and each site can accommodate only one molecule or ion. The adsorbed ions cannot migrate across the surface or interact with neighboring molecules. The results by the Langmuir isotherm modeling are shown in Fig. 6. The parameters results by the Langmuir isotherm modeling are listed in Table 3. The adsorbed Hg(II) may be considered to form a tetrahedral complex as $[Hg(OH)_2(H_2O)_2]$ [50]. The Langmuir maximum adsorption capacity (Q^0) decreased with increasing the temperatures, which reflects the exothermic nature of the physical adsorption. The results show that the adsorption isotherm equilibrium of Hg(II) on the TiO_2 nanoparticles and the TiO_2/montmorillonite can be described well by the Langmuir adsorption model.

The kinetic process of adsorption of Hg(II) on solid materials may be described by the Elovich equation, which was established by the work of Zeldowitsch in 1934. In earlier years, the equation has been widely used to describe the kinetics of adsorption of gases onto solids [51]. Recently, the Elovich equation has also been used extensively to describe the adsorption of pollutants from aqueous solutions on solids especially when the adsorption rate decreases with time due to an increased surface coverage of the material [52–55].

$$\frac{dq_t}{dt} = \alpha \exp(-\beta q_t) \tag{3}$$

where q_t (mg g^{-1}) is the amount of Hg(II) adsorption at time t (min), α (mg g^{-1} min^{-1}) is related to the initial adsorption rate, β (g mg^{-1}) is the constant related to the surface coverage of the materials.

To simplify Elovich's equation, some researchers assumed $t >> (1/\alpha\beta)$ and by applying the boundary conditions of $q_t = 0$ at $t = 0$ and $q_t = q_t$ at $t = t$, then Eq. (3) becomes [52–58]:

$$q_t = \left(\frac{1}{\beta}\right) \ln(\alpha\beta) + \frac{1}{\beta} \ln(t) \tag{4}$$

The amount of Hg(II) adsorbed onto the materials, q_t was found by a mass balance relationship:

$$q_t = (c_0 - c)\frac{V}{W} \tag{5}$$

where V (l) is the volume of the solution and W (mg) the mass of the corresponding solid sample.

Eq. (6) can be obtained:

$$\frac{c}{c_0} = \varphi \ln(t) + \theta \tag{6}$$

where $\varphi = -\frac{W}{\beta c_0 V}$; $\theta = 1 - \frac{W}{\beta c_0 V} \ln(\alpha\beta)$

The linear relationship of c/c_0 and $\ln t$ is shown in Fig. 7, and the parameters of the Elovich equation including α, β, and the correlation coefficient (R) are presented in Table 4. The results show that the Elovich equation can describe this process well. The assumption $t >> (1/\alpha\beta)$ is justified and the value of α for TiO_2/montmorillonite is larger at a given temperature than that for the TiO_2 nanoparticles, which indicates a higher rate of adsorption using TiO_2/montmorillonite.

Table 3
Langmuir parameters corresponding to the fitting of the experimental equilibrium data.

Materials	T (°C)	Q^0 (mg g^{-1})	K_L (l mg^{-1})	r	R
TiO_2 nanoparticles	25	101.1	0.0056	0.641	0.99993
	35	98.1	0.0053	0.654	0.99901
	45	90.4	0.0051	0.662	0.99854
TiO_2/montmorillonite	25	123.8	0.0054	0.650	0.99531
	35	118.3	0.0044	0.694	0.99889
	45	116.5	0.0037	0.730	0.99995

3.3.2. Photocatalytic reduction of Hg(II)

With the UV illumination, when TiO_2 materials were added into Hg(II) solutions the white TiO_2 turned black with time, indicating Hg was produced. The time profiles of Hg(II) photo-reduction catalyzed by the TiO_2 nanoparticles and TiO_2/montmorillonite samples are presented in Fig. 8. The removal of Hg(II) in aqueous solutions increased with increasing temperatures, and under

Table 4
Parameters of Elovich equation.

Samples	T (°C)	R	φ	θ	α (mg g^{-1} min^{-1})	β ($\times 10^{-2}$) (g mg^{-1})
TiO_2 nanoparticles	25	0.9940	−0.359	1.976	54.4	2.79
	35	0.9906	−0.329	1.908	48.8	3.03
	45	0.9944	−0.288	1.803	41.8	3.47
TiO_2/montmorillonite	25	0.9935	−0.396	2.029	65.5	2.52
	35	0.9960	−0.373	1.995	58.6	2.68
	45	0.9886	−0.355	1.979	52.3	2.82

the 90 min UV illumination at 45 °C, decrease percentages of more than 80% and 90% Hg(II) were achieved with the synthesized TiO_2 nanoparticles and TiO_2/montmorillonite, respectively. Hg(II) concentration in the liquid solutions remained almost constant after 50 min. The dispersed titanium oxides deposited on the surface of montmorillonite or included in layers cavities were used as the photocatalyst showing high efficiency of Hg(II) removal in aqueous solutions. The study explained there may be due to catalysts having a tetrahedral coordination; resulting in high, characteristic photocatalytic reactivity compared to that of the bulk TiO_2 powder catalyst [59]. Considering the influence of the reduction reaction of Hg(II) on catalyst activity, the activity may be high during the initial period. The metallic mercury was then produced and could deposit on the surface of solids resulting in a decrease in catalyst activity.

The overall process of photocatalytic reduction can also be decomposed into several steps including: (a), transfer of the reactants in the fluid phase to the surface; (b), adsorption of the reactants; (c), reaction in the adsorbed phase; (d), desorption of the product; (e), removal of the product from the interface region. The photocatalytic reaction occurs in the adsorbed phase [6]. In the presence of a photocatalyst and UV illumination, Hg(II) can be reduced to Hg by the excited electrons. For $HgCl_2$, some possible hydrolytic effects take place:

$$HgCl_2 + H_2O \rightarrow Hg(OH)Cl + H^+ + Cl^- \quad (R3)$$

This hydrolytic effect could inhibit the photocatalytic reduction of mercury(II), and the mechanism for Cl^- in inhibiting photocatalysis via hydroxyl radical and holes scavenging was proposed [60]:

$$cl^- + OH^\bullet \rightarrow cl^\bullet + OH^- \quad (R4)$$

$$cl^- + h^+ \rightarrow cl^\bullet \quad (R5)$$

The Cl^- accounted for its inhibitory effect on TiO_2 photocatalysis through a preferential adsorption displacement mechanism over the surface bound OH^- ions. This reduces the number of OH^-

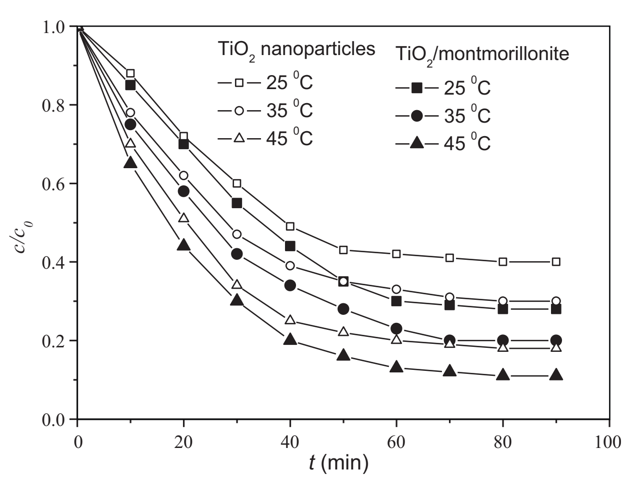

Fig. 8. Decreasing Hg(II) concentrations with time by photocatalytic reduction at the different temperatures in aqueous solutions.

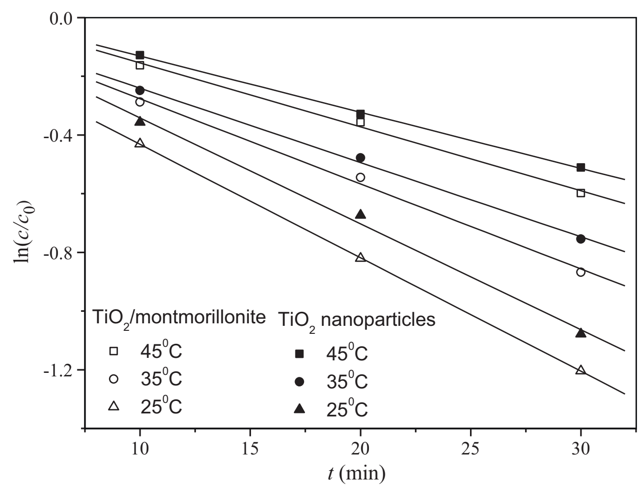

Fig. 9. Relationship between $\ln(c/c_0)$ and t at the different temperatures during photocatalytic reduction of Hg(II) for the initial time of 30 min.

ions available on the TiO_2 surface, and the substituted Cl^- further increases the recombination of electronehole pairs [60]. The study showed a significant decrease in the photo-reduction rate of Hg(II) as chloride concentration increased, and some species including $HgCl_2$, $HgCl^+$, $HgCl_3{}^-$, and $HgCl_4{}^{2-}$ could be formed in the excess of Cl^- in water [2].

We can illustrate the method of data interpretation with a kinetic model for photocatalytic reaction assuming a first order kinetic model for the reaction rate [5,33]:

$$c = c_0 \exp(-k_A t) \quad (8)$$

where k_A is the apparent kinetic constant.

The effect of temperature on k_A can also be obtained by changing the temperatures of solutions, and the activation energy for the photocatalytic reduction reaction was further determined by using the following Arrhenius equations:

$$k_A = k_0 \exp\left(-\frac{E_A}{RT}\right) \quad (9)$$

where k_0 is the frequency factor.

The relationship between $\ln(c/c_0)$ and t at the different temperatures during photocatalytic reduction of Hg(II) is shown in Fig. 9 for the initial time of 30 min. As shown in Fig. 9, the kinetic model with the first-order reaction was in excellent agreement with the experimental data. The determined parameters of activation energy and pre-exponential factor are given in Table 5. The apparent activation energies of 25.0 and 22.6 kJ mol^{-1} in Table 5 are in agreement with the reported value range for Hg(II) photoreduction using pho-

Table 5
Activation energies and pre-exponential factors.

Material	R	E_A (kJ mol^{-1})	k_0 (min^{-1})
TiO_2 nanoparticles	0.9962	25.0	2.4×10^{-4}
TiO_2/montmorillonite	0.9998	22.6	9.3×10^{-5}

tocatalysts, and some studies also indicated the 10–40 kJ mol^{-1} for photocatalysts [6].

4. Conclusions

In this work, we have demonstrated some approaches to the synthesis of TiO_2 nanoparticles and of TiO_2/montmorillonite, and to the removal of toxic Hg(II) in aqueous solutions both by the adsorption and photocatalytic reaction at different temperatures. It was found that the TiO_2 nanoparticles had a narrow size distribution, and the average particles diameter was 9.1 nm. The TiO_2/montmorillonite exhibited the highest specific surface area of 239 m^2 g^{-1} and average pore diameter of 3.10 nm. High purity anatase TiO_2 nanoparticles were produced by heat treatment at 500 °C. The experiments were carried out to test the removal of Hg(II) in aqueous solutions from 25 °C to 45 °C. The results showed that the concentrations of Hg(II) in aqueous solutions increased with increasing temperature within the stated range, indicating a decrease in the adsorption process. TiO_2/montmorillonite exhibiting TiO_2 clusters introduced (and attached) in the montmorillonite is found to behave differently from bulk TiO_2 and exhibit excellent catalytic and adsorption properties. The adsorption of Hg(II) on the materials was described by the Langmuir isotherm model and the kinetics were given by the Elovich equation. A kinetic model of a first-order reaction simulated the photocatalytic reduction rate with a good fit, and the activation energies and pre-exponential factors were calculated according to the Arrhenius equation.

Acknowledgements

This work was supported by the Science and Technology Commission of Shanghai Municipality (07DZ12013). The work is supported by the Fundamental Research Funds for the Central Universities (3003-893331).

References

[1] R. Herrero, P. Lodeiro, C. Rey-Castro, T. Vilarino, D.S. Vicente, Removal of inorganic mercury from aqueous solutions by biomass of the marine macroalga Cystoseira baccata, Water Res. 39 (2005) 3199–3210.

[2] X.L. Wang, S.O. Pehkonen, A.K. Ray, Photocatalytic reduction of Hg(II) on two commercial TiO_2 catalysts, Electrochim. Acta 49 (2004) 1435–1444.

[3] K.P. Lisha, M. Shihabudheen, T. Maliyekkal, Pradeep, Manganese dioxide nanowhiskers: a potential adsorbent for the removal of Hg(II) from water, Chem. Eng. J. 160 (2010) 432–439.

[4] H. Bessbousse, T. Rhlalou, J.-F. Verchère, L. Lebrun, Mercury removal from wastewater using a poly(vinylalcohol)/poly(vinylimidazole) complexing membrane, Chem. Eng. J. 164 (2010) 37–48.

[5] L.B. Khalil, M.W. Rophael, W.E. Mourad, The removal of the toxic Hg(II) salts from water by photocatalysis, Appl. Catal. B: Environ. 36 (2002) 125–130.

[6] L.R. Skubal, N.K. Meshkov, Reduction and removal of mercury from water using arginine-modified TiO_2, J. Photochem. Photobiol. A: Chem. 148 (2002) 211–214.

[7] J. Hegyi, O. Horvath, Photocatalytic reduction of mercury(II) and simultaneous oxidative degradation of surfactants in titanium dioxide suspensions, Prog. Colloid Polym. Sci. 125 (2004) 10–16.

[8] O. Horváth, J. Hegyi, Light-induced reduction of heavy-metal ions on titanium dioxide dispersions, Prog. Colloid Polym. Sci. 117 (2002) 211–216.

[9] M. Hussain, R. Ceccarelli, D.L. Marchisio, D. Fino, N. Russo, F. Geobaldo, Synthesis, characterization, and photocatalytic application of novel TiO_2 nanoparticles, Chem. Eng. J. 157 (2010) 45–51.

[10] C. Sriwong, S. Wongnawa, O. Patarapaiboolchai, Photocatalytic activity of rubber sheet impregnated with TiO_2 particles and its recyclability, Catal. Commun. 9 (2008) 213–218.

[11] M. Saquib, M.A. Tariq, M. Faisal, M. Muneer, Photocatalytic degradation of two selected dye derivatives in aqueous suspensions of titanium dioxide, Desalination 219 (2008) 301–311.

[12] M.C. Hidalgo, M. Aguilar, M. Maicu, J.A. Navıo, G. Colon, Hydrothermal preparation of highly photoactive TiO_2 nanoparticles, Catal. Today 129 (2007) 50–58.

[13] S.W. Oh, S.H. Park, Y.K. Sun, Hydrothermal synthesis of nano-sized anatase TiO_2 powders for lithium secondary anode materials, J. Power Sources 161 (2006) 1314–1318.

[14] F. Sayılkan, S. Erdemoğlu, M. Asiltürk, M. Akarsu, S. Şener, S. Sayılkan, S. Erdemoğlu, E. Arpaç, Photocatalytic performance of pure anatase nanocrystallite TiO_2 synthesized under low temperature hydrothermal conditions, Mater. Res. Bull. 41 (2006) 2276–2285.

[15] T. Chou, T. Ling, M. Yang, C. Liu, Micro and nano scale metal oxide hollow particles produced by spray precipitation in a liquid–liquid system, Mater. Sci. Eng. A 359 (2006) 24–30.

[16] A.R. Rao, V. Dutta, Low-temperature synthesis of TiO_2 nanoparticles and preparation of TiO_2 thin films by spray deposition, Sol. Energy Mater. Sol. C 91 (2007) 1075–1080.

[17] K. Nagaveni, G. Sivalingam, M. Hegde, G. Madras, Photocatalytic degradation of organic compounds over combustion-synthesized nano-TiO_2, Environ. Sci. Technol. 38 (2004) 1600–1604.

[18] T. Sahm, L. Mädler, A. Gurlo, N. Barsan, S.E. Pratsinis, U. Weimar, Flame spray synthesis of tin dioxide nanoparticles for gas sensing, Sens. Actuators B: Chem. 98 (2004) 148–153.

[19] M. Crişan, A. Brăileanu, M. Răileanu, M. Zaharescu, D. Crişan, N. Drăgan, M. Anastasescu, A. Ianculescu, I. Niţoi, V.E. Marinescu, S.M. Hodorogea, Sol–gel S-doped TiO_2 materials for environmental protection, J. Non-Cryst. Solid 354 (2008) 705–711.

[20] R.S. Sonawane, S.G. Hegde, M.K. Dongare, Preparation of titanium(IV) oxide thin film photocatalyst by sol–gel dip coating, Mater. Chem. Phys. 77 (2003) 744–750.

[21] N.B. Shali, S. Sugunan, Influence of calcination ambient and film thickness on the optical and structural properties of sol–gel TiO_2 thin films, Mater. Res. Bull. 42 (2007) 1777–1783.

[22] C. Wu, J. Huang, J. Wen, S. Wen, Y. Shen, M. Yeh, Preparation of TiO_2 nanoparticles by supercritical carbon dioxide, Mater. Lett. 62 (2008) 1923–1926.

[23] P.P. Ahonen, U. Tapper, E.I. Kauppinen, J. Joubert, J. Deschanvres, Aerosol synthesis of Ti–O powders via in-droplet hydrolysis of titanium alkoxide, Mater. Sci. Eng. A 315 (2001) 113–121.

[24] M. Kanna, S. Wongnawa, Mixed amorphous and nanocrystalline TiO_2 powders prepared by sol–gel method: characterization and photocatalytic study, Mater. Chem. Phys. 110 (2008) 166–175.

[25] G. Chen, G. Luo, J. Xu, J. Wang, Membrane dispersion precipitation method to prepare nanopartials, Powder Technol. 139 (2004) 180–185.

[26] S. Mahshid, M. Askari, M. Ghamsari, Synthesis of TiO_2 nanoparticles by hydrolysis and peptization of titanium isopropoxide solution, J. Mater. Process. Technol. 189 (2007) 296–300.

[27] V. Belessi, D. Lambropoulou, I. Konstantinou, A. Katsoulidis, P. Pomonis, D. Petridis, T. Albanis, Structure and photocatalytic performance of TiO_2/clay nanocomposites for the degradation of dimethachlor, Appl. Catal. B: Environ. 73 (2007) 292–299.

[28] X. Ding, T. An, G. Li, S. Zhang, J. Chen, J. Yuan, J. Zhao, H. Chen, G. Sheng, J. Fu, Preparation and characterization of hydrophobic TiO_2 pillared clay: the effect of acid hydrolysis catalyst and doped Pt amount on photocatalytic activity, J. Colloid Interface Sci. 320 (2008) 501–507.

[29] Y. Gao, Y. Masuda, W. Seo, H. Ohta, H. Koumoto, TiO_2 nanoparticles prepared using an aqueous peroxotitanate solution, Ceram. Int. 30 (2004) 1365–1368.

[30] A. Fernández, G. Lassaletta, V.M. Jiménez, A. Justo, A.R. González-Elipe, J.M. Herrmann, H. Tahiri, Y. Ait-Ichou, Preparation and characterization of TiO_2 photocatalysts supported on various rigid supports (glass, quartz and stainless steel). Comparative studies of photocatalytic activity in water purification, Appl. Catal. B: Environ. 7 (1995) 49–63.

[31] R. Kun, K. Mogyorósi, I. Dékány, Synthesis and structural and photocatalytic properties of TiO_2/montmorillonite nanocomposites, Appl. Clay Sci. 32 (2006) 99–110.

[32] K. Shimizu, T. Kaneko, T. Fujishima, T. Kodama, H. Yoshida, Y. Kitayama, Selective oxidation of liquid hydrocarbons over photoirradiated TiO_2 pillared clays, Appl. Catal. A: Gen. 225 (2002) 185–188.

[33] J. Yang, J. Zhang, L. Zhu, S. Chen, Y. Zhang, Y. Tang, Y. Zhua, Y. Li, Synthesis of nano titania particles embedded in mesoporous SBA-15: characterization and photocatalytic activity, J. Hazard. Mater. B137 (2006) 952–958.

[34] G. Li, X. Zhao, M. Ray, Advanced oxidation of orange II using TiO_2 supported on porous adsorbents: the role of pH, H_2O_2 and O_3, Sep. Purif. Technol. 55 (2007) 91–97.

[35] S. Doeuff, M. Henry, C. Sanchez, J. Livage, Hydrolysis of titanium alkoxides: modification of the molecular precursor by acetic acid, J. Non-Cryst. Solid 89 (1987) 206–216.

[36] W. Guo, Z. Lin, X. Wang, G. Song, Sonochemical synthesis of nanocrystalline TiO_2 by hydrolysis of titanium alkoxides, Microelectron. Eng. 66 (2003) 95–101.

[37] J. Liu, M. Dong, S. Zuo, Y. Yu, Solvothermal preparation of TiO_2/montmorillonite and photocatalytic activity, Appl. Clay Sci. 43 (2009) 156–159.

[38] L. Yan, J. Wang, H. Yu, Q. Wei, B. Du, X. Shan, Adsorption of benzoic acid by CTAB exchanged montmorillonite, Appl. Clay Sci. 37 (2007) 226–230.

[39] Y. Ku, W.H. Lee, W.Y. Wang, Photocatalytic reduction of carbonate in aqueous solution by UV/TiO_2 process, J. Mol. Catal. A: Chem. 212 (2004) 191–196.

[40] O.S. Ahmed, D.K. Dutt, In situ generation of metal clusters in interlamellar spacing of montmorillonite clay and their thermal behavior, Thermochim. Acta 395 (2002) 209–216.

[41] L. Xiang, X. Zhao, Preparation of montmorillonite/titania nanocomposite and enhanced electrorheological activity, J. Colloid Interface Sci. 296 (2006) 131–140.

[42] T. Sugimoto, X. Zhou, Synthesis of uniform anatase TiO_2 nanoparticles by the gel–sol method: 2. Adsorption of OH-ions to $Ti(OH)_4$ gel and TiO_2 particles, J. Colloid Interface Sci. 252 (2002) 347–353.

[43] J.T. Banks, T. Yu, H. Yu, Direct visualization of the hydrolysis kinetics of titanium(IV) alkoxides on functionalized gold surfaces, J. Phys. Chem. B 106 (2002) 3538–3542.

[44] I. Zuo, C. Nie, X. Gu, Y. Lai, Y. Zong, L. Sun, C. Lin, Fabrication of TiO_2/Au nanorod arrays employing a positive sacrificial ZnO template and their electrochromic property, Mater. Lett. 61 (2007) 2632–2637.

[45] P. Yuan, X. Yin, H. He, D. Yang, L. Wang, J. Zhu, Investigation on the delaminated-pillared structure of TiO_2-PILC synthesized by $TiCl_4$ hydrolysis method, Microporous Mesoporous Mater. 93 (2006) 240–247.

[46] S. Yamanaka, T. Nishihara, M. Hattori, Y. Suzuki, Preparation and properties of titania pillared clay, Mater. Chem. Phys. 17 (1987) 87–101.

[47] S.G. Hur, T. Kim, S. Hwang, S. Hwang, J. Yang, J. Choy, Heterostructured nanohybrid of zinc oxide-montmorillonite clay, J. Phys. Chem. B 110 (2006) 1599–1604.

[48] K.O. Adebowale, I.E. Unuabonah, B.I. Olu-Owolabi, The effect of some operating variables on the adsorption of lead and cadmium ions on kaolinite clay, J. Hazard. Mater. B134 (2006) 130–139.

[49] F. Rozada, M. Otero, A. Moran, A. Garcıa, Adsorption of heavy metals onto sewage sludge-derived materials, Bioresour. Technol. 99 (2008) 6332–6338.

[50] M. Aguado, S. Cervera-March, J. Giménez, Continuous photocatalytic treatment of mercury(II) on titania powders. Kinetics and catalyst activity, Chem. Eng. Sci. 50 (1995) 1561–1569.

[51] N.H. Turner, Kinetics of chemisorption: an examination of the Elovich equation, J. Catal. 36 (1975) 262–265.

[52] Y. Ho, Review of second-order models for adsorption systems, J. Hazard. Mater. 136 (2006) 681–689.

[53] A. Gunay, E. Arslankaya, I. Tosun, Lead removal from aqueous solution by natural and pretreated clinoptilolite: adsorption equilibrium and kinetics, J. Hazard. Mater. 146 (2007) 362–371.

[54] M. Alkan, M. Doğan, Y. Turhan, Q. mirbaş, P. Turan, Adsorption kinetics and mechanism of maxilon blue 5G dye on sepiolite from aqueous solutions, Chem. Eng. J. 139 (2008) 213–223.

[55] C.O. Illanes, N.A. Ochoa, J. Marchese, Kinetic sorption of Cr(VI) into solvent impregnated porous microspheres, Chem. Eng. J. 136 (2008) 92–98.

[56] S.H. Chien, W.R. Clayton, Application of Elovich equation to the kinetics of phosphate release and sorption in soils, Soil Sci. Soc. Am. J. 44 (1980) 265–268.

[57] Y.S. Ho, G. McKay, A comparison of chemisorption kinetic models applied to pollutant removal on various sorbents, Process Saf. Environ. Protect. 76B (1998) 332–340.

[58] R. Tseng, F. Wu, R. Juang, Liquid-phase adsorption of dyes and phenols using pinewood-based activated carbons, Carbon 41 (2003) 487–495.

[59] S. Anandan, M. Yoon, Photocatalytic activities of the nano-sized TiO_2-supported Y-zeolites, J. Photochem. Photobiol. C: Photochem. Rev. 4 (2003) 5–18.

[60] M.N. Chong, B. Jin, C.W.K. Chow, C. Saint, Recent developments in photocatalytic water treatment technology: a review, Water Res. 44 (2010) 2997–3027.